

Comparison of Time Domain Numerical Solvers for the Propagation of a Gaussian Pulse Inside a Rectangular Waveguide

V.Vegh and I. W. Turner
School of Mathematical Sciences
Centre in Statistical Science and Industrial Mathematics
Queensland University of Technology
GPO Box 2324
Brisbane Q4001 Australia
e-mail: v.vegh@qut.edu.au, i.turner@fsc.qut.edu.au

Abstract

This research work analyses techniques for increasing the accuracy and efficiency of a finite-volume time-domain (FV-TD) cell-centred computational methodology. Various state-of-the-art spatial and temporal discretisation methods employed to solve Maxwell equations on multi-dimensional structured grid networks are investigated and the dispersive and dissipative errors inherent in those techniques examined. Both staggered and unstaggered grid approaches are considered. Staggered and unstaggered Leapfrog and Runge-Kutta time integration methods are analysed by the use of Gaussian microwave pulse simulations. The implementation of typical electromagnetic boundary conditions is also deliberated. Finally, a comparison of the classical finite-difference time-domain (FD-TD) method and FV-TD numerical results for a standard case study in rectangular waveguides allows the accuracy of the developed methods to be assessed.

Introduction

In the past, a number of computational methodologies have been developed for the solution of Maxwell Equations for a variety of important applications in Science and Engineering [1-4]. Although microwaves are frequently used for heating purposes, in this paper only microwave pulses are analysed for the purpose of radar and signal processing. In the past, research work in Computational Electromagnetics (CEM) has seen the development of approximations both for the integral and point forms of the governing Maxwell's equations. In this work on structured grids, the traditional staggered in time and space FD-TD [5] scheme is compared to a number of cell-centred finite-volume time-domain approaches (ccFV-TD). Most of the schemes discussed here are formulated for generalised unstructured applications, however, at this stage of the research work are implemented on a simpler structured mesh case study, so that the results can be compared directly with the FD-TD solution.

Inside a finite-volume cell within the computational domain, staggered schemes store approximations of the components of the electromagnetic fields at different spatial locations in space. For example, FD-TD uses the Yee lattice to achieve that objective, as in Fig. 1. In

this case, the electric and magnetic fields are staggered also in time in order to stabilise the explicit time marching scheme. On the contrary, cell-centred schemes store all of the electromagnetic fields at the same spatial location (ie. the cell centre). Typically, cell-centred schemes are much easier to manage and implement (in terms of algorithm planning, design and storage data structures) in comparison with their staggered counterparts. Note however that even though the electric and magnetic field components are evaluated at the same locations inside a given cell, it is still possible to stagger the cell-centred in space schemes in time. These are usually classified as staggered and unstaggered leapfrog integrations in time, where the electric and magnetic field components are either stored at different locations or at the same location in time, respectively.

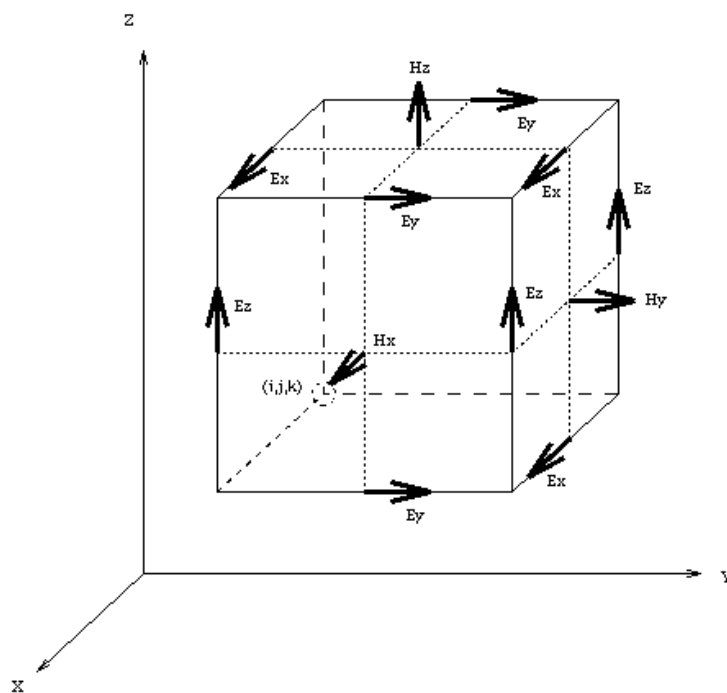


Figure 1. A Yee cell. The components of the electric (E) and magnetic (H) fields are stored at different locations along the cell edges and on the cell faces, respectively. For the FD-TD algorithm, the electric and magnetic fields are also half a time step apart.

In this work, 3rd and 4th order Runge-Kutta (RK3 and RK4) methods are implemented also on the cell-centred in space approach to analyse their performance, compared with the Leapfrog time marching schemes.

The problem under study here concerns a TE₁₀ Gaussian pulse propagated longitudinally in a typical rectangular waveguide. The end of the waveguide is short-circuited, and the reflected waves are absorbed in the scattered field region of the waveguide. Initially, a detailed description of the mathematical formulation is provided for the time domain cell-centred in space methods, and typical boundary condition implementation for the conducting walls, input plane and absorbing boundary layer is deliberated. In the scattered field region of the waveguide, an existing Perfectly Matched Layer (PML) staggered in space methodology [6] is adapted to the cell-centred approaches to absorb any reflected impinging waves in the scattered field region of the waveguide.

Primarily, the propagating Gaussian pulse empty waveguide study allows the performance of the different Maxwell's equations time domain solvers to be analysed under free space conditions. The pulse presents a good test for the FV-TD methods, and highlights the evident dissimilarities between the different cell-centred schemes and shows also, the differences when compared to the FD-TD method. Depending on the spatial and temporal discretisation methods utilised, the schemes exhibit both dispersive and dissipative numerical errors. Dissipative errors cause the loss of wave amplitude, while dispersive errors affect the wave propagation speed. These errors are cumulative in nature and need to be monitored for a number of time steps.

This paper is broken up as follows. In the next section the mathematical formulation for discretising Maxwell's equations using a finite-volume approach is presented, highlighting the different cell-centred schemes. Then there follows a detailed discussion of the electromagnetic boundary condition implementation. In the proceeding section the results for the empty waveguide case study are presented, and comparisons between the different methods are provided via a number of graphical illustrations that elucidate the dissipative and dispersive nature of the different schemes. Finally, the conclusions of this work are summarised.

Cell-Centred Finite-Volume Time-Domain Methods

For the purpose of numerical simulation using a finite-volume methodology, the point form of the Maxwell equations (1) must be recast into a discrete volumetric form:

$$\nabla \times \mathbf{E} = -\frac{\partial \mathbf{B}}{\partial t}, \quad \nabla \times \mathbf{B} = \frac{\partial \mathbf{D}}{\partial t} + \mathbf{J}, \quad (1)$$

$$\mathbf{B} = \mu_0 \mathbf{H}, \quad \mathbf{D} = \varepsilon \mathbf{E}, \quad \mathbf{J} = \sigma \mathbf{E}, \quad \varepsilon = \varepsilon_0 \varepsilon', \quad \sigma = \omega \varepsilon_0 \varepsilon''.$$

To arrive at the volumetric form, integration over a discrete finite volume cell is carried out. Unlike previous techniques where the integral was approximated using Stokes' theorem [3, 7], the Divergence theorem is applied to the volumetric representation to obtain a surface-volume relationship between the electric and magnetic fields. The continuous equation is then cast into discrete form as follows:

$$\frac{\partial \mathbf{B}_p}{\partial t} = -\frac{1}{\Delta V} \sum_{F \in \zeta_p} \mathbf{n} \times \mathbf{E}_F \Delta S_F, \quad \frac{\partial \mathbf{D}_p}{\partial t} = \frac{1}{\Delta V} \sum_{F \in \zeta_p} \mathbf{n} \times \mathbf{H}_F \Delta S_F - \mathbf{J}_p. \quad (2)$$

where, \mathbf{n} is the unit outward normal through a face of a particular cell (see Fig. 2). In the equations, ζ_p is the set of faces that constitute the p^{th} cell in a computational domain. ΔS_F and ΔV are the surface area of a particular face in ζ_p and the volume of the p^{th} cell, respectively. For the above discrete representation of Maxwell's equations (2), the surface integral approximation is second order in space if \mathbf{E}_F and \mathbf{H}_F are the values at the midpoint of the face. By visiting all of the cells that constitute the solution domain, a system of ordinary differential equations (ODEs) results. A number of methods are proposed to resolve the system of ODEs.

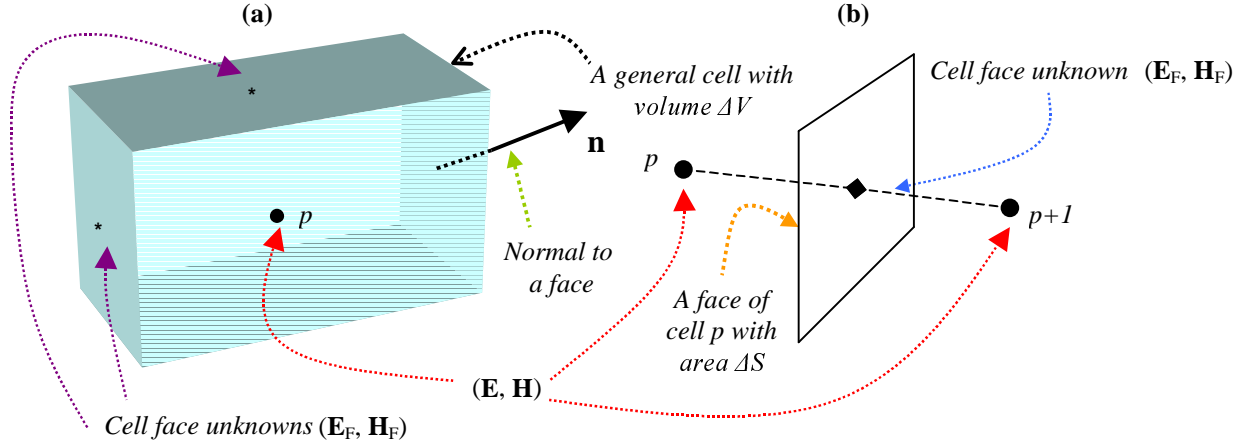


Figure 2. A general cell within a computational domain with the locations of the unknowns.

When approximating the differential operator in time, the discretisation can introduce either dispersion or dissipation errors (see [4]). Numerous techniques can be utilised to resolve (2) into time discrete form. In [8] a number of approaches similar to the FD-TD solution methodology have been investigated. For a function φ , equations (3a) and (3b) are the staggered (SLF) and unstaggered (ULF) leapfrog discretisations respectively. Both the staggered and unstaggered approximations are $O(\Delta t^2)$:

$$\frac{\partial \varphi^{n+\frac{1}{2}}}{\partial t} = \frac{\varphi^{n+1} - \varphi^n}{\Delta t}, \quad (3a)$$

$$\frac{\partial \varphi^n}{\partial t} = \frac{\varphi^{n+1} - \varphi^{n-1}}{2\Delta t}. \quad (3b)$$

Methods using the discretisations in (3) have been used in the past to numerically solve for the electromagnetic fields governed by Maxwell's equations. Using (3a), equation (2) is written in discrete form as:

$$\mathbf{H}_p^{n+\frac{1}{2}} = \mathbf{H}_p^{n-\frac{1}{2}} - \frac{\Delta t}{\mu_0 \Delta V} \sum_{F \in \zeta_p} \mathbf{n} \times (\mathbf{E}_F)^n \Delta S_F, \quad (4a)$$

$$\mathbf{E}_p^{n+1} = \frac{2\varepsilon - \sigma \Delta t}{2\varepsilon + \sigma \Delta t} \mathbf{E}_p^n + \frac{2\Delta t}{(2\varepsilon + \sigma \Delta t) \Delta V} \sum_{F \in \zeta_p} \mathbf{n} \times (\mathbf{H}_F)^{n+\frac{1}{2}} \Delta S_F. \quad (4b)$$

Similarly, (2) with the substitution of the discretisation in (3b) becomes:

$$\mathbf{H}_p^{n+1} = \mathbf{H}_p^{n-1} - \frac{2\Delta t}{\mu_0 \Delta V} \sum_{F \in \zeta_p} \mathbf{n} \times (\mathbf{E}_F)^n \Delta S_F, \quad (5a)$$

$$\mathbf{E}_p^{n+1} = \frac{\varepsilon - \sigma \Delta t}{\varepsilon + \sigma \Delta t} \mathbf{E}_p^{n-1} + \frac{2\Delta t}{(\varepsilon + \sigma \Delta t) \Delta V} \sum_{F \in \zeta_p} \mathbf{n} \times (\mathbf{H}_F)^n \Delta S_F. \quad (5b)$$

Equation (4) and (5) require the approximation to the electric and magnetic fields at the cell faces. It is possible to propose a number of interpolating and extrapolating schemes to approximate these cell face unknowns. On structured grids, the simplest way to approximate the unknowns at a cell face is by averaging the cell values about a particular face. Such a

technique imposes second order in space and time for (4) and (5). These particular finite-volume methods will be referred to as SLF (4), staggered in time and unstaggered in space, and ULF (5), unstaggered in space and unstaggered in time Leapfrog discretisations.

The averaging about a cell face demonstrates the simplest way to approximate the terms inside the summations in (4) and (5). At the p^{th} cell in (2), Intensity-Vector Splitting (IVS) [4], which is a concept that originated from Computational Fluid Dynamics (CFD), can be applied to replace the $\mathbf{n} \times \mathbf{E}_F$ and $\mathbf{n} \times \mathbf{H}_F$ terms of equations (4) and (5). The notion behind IVS is to include an extra term in the flux facial expression to dampen any numerical oscillations, and to capture any discontinuities (such as shocks and contact surfaces in CFD) in the solution. At a cell face F , equation (6) depicts the derived form of the IVS result:

$$\mathbf{n} \times \mathbf{E}_F = \frac{1}{2} \mathbf{n} \times (\mathbf{E}_F^+ + \mathbf{E}_F^-) + \frac{1}{2} \mathbf{n} \times \left\{ [\mu c]^+ \mathbf{n} \times \mathbf{H}_F^+ - [\mu c]^- \mathbf{n} \times \mathbf{H}_F^- \right\}, \quad (6a)$$

$$\mathbf{n} \times \mathbf{H}_F = \frac{1}{2} \mathbf{n} \times (\mathbf{H}_F^+ + \mathbf{H}_F^-) - \frac{1}{2} \mathbf{n} \times \left\{ [\epsilon c]^+ \mathbf{n} \times \mathbf{E}_F^+ - [\epsilon c]^- \mathbf{n} \times \mathbf{E}_F^- \right\}. \quad (6b)$$

where, the wave speed is given by $c = 1/\sqrt{\mu\epsilon}$. It is evident from (6) that the + and – characteristics have to be approximated for a given cell face. It should be noted that the IVS result cannot be implemented with (3a), since the values for the magnetic and electric fields are required at different time levels. For this reason, time marching schemes that allow the electric and magnetic field components to be located at the same instant in time have to be employed. Numerical experimentation has shown that IVS when incorporated with (3b) incurs large errors due to the time discretisation of the electric and magnetic fields [4]. Therefore, higher order time stepping methods are to be implemented. The following 3rd order Runge-Kutta (RK3) method was implemented with the IVS scheme discussed above:

$$\begin{aligned} \varphi^{n+\frac{1}{3}} &= \varphi^n + \frac{\Delta t}{3} \frac{\partial \varphi^n}{\partial t}, & \varphi^{n+\frac{2}{3}} &= \varphi^n + \frac{2\Delta t}{3} \frac{\partial \varphi^{n+\frac{1}{3}}}{\partial t}, \\ \varphi^{n+1} &= \varphi^n + \frac{\Delta t}{4} \left(3 \frac{\partial \varphi^{n+\frac{2}{3}}}{\partial t} + \frac{\partial \varphi^n}{\partial t} \right). \end{aligned} \quad (7)$$

The outlined RK3 scheme is the one commonly used in CEM, and hence, it was chosen to solve the equations of (2) that employ (6). Also, a 4th order Runge-Kutta (RK4) method was implemented:

$$\begin{aligned} \hat{\varphi}^{n+\frac{1}{2}} &= \varphi^n + \frac{\Delta t}{2} \frac{\partial \varphi^n}{\partial t}, & \tilde{\varphi}^{n+\frac{1}{2}} &= \varphi^n + \frac{\Delta t}{2} \frac{\partial \hat{\varphi}^{n+\frac{1}{2}}}{\partial t}, \\ \bar{\varphi}^{n+1} &= \varphi^n + \Delta t \frac{\partial \tilde{\varphi}^{n+\frac{1}{2}}}{\partial t}, & \varphi^{n+1} &= \varphi^n + \frac{\Delta t}{6} \left(\frac{\partial \varphi^n}{\partial t} + 2 \frac{\partial \hat{\varphi}^{n+\frac{1}{2}}}{\partial t} + 2 \frac{\partial \tilde{\varphi}^{n+\frac{1}{2}}}{\partial t} + \frac{\partial \bar{\varphi}^{n+1}}{\partial t} \right). \end{aligned} \quad (8)$$

Substituting the IVS result into (2) and by applying the RK solvers of (7) and (8), the RK3-IVS and RK4-IVS techniques are obtained, respectively. Note that (2) can be solved using the RK3 and RK4 solvers without the inclusion of damping, and this suggestion is pursued later in this section.

As shown in Fig. 2, the + and – characteristics for the IVS are required at a particular cell face. Different strategies can be proposed and derived to approximate the values at the cell

face joining any two adjacent cells. The simplest of these is the 0th order substitution for an unknown ξ :

$$\xi_{p+\frac{1}{2}}^- = \xi_p, \quad \xi_{p+\frac{1}{2}}^+ = \xi_{p+1}. \quad (9)$$

Imposing the 0th order approximation in RK3-IVS and RK4-IVS leads to a 1st order in space and 3rd order in time RK3-1-IVS numerical method, and a 1st order in space and 4th order in time RK4-1-IVS numerical method respectively. On a structured grid, a general linear extrapolation model that is 2nd order in space can also be derived:

$$\xi_{p+\frac{1}{2}}^- = \frac{1}{2}(3\xi_p - \xi_{p-1}), \quad \xi_{p+\frac{1}{2}}^+ = \frac{1}{2}(3\xi_{p+1} - \xi_{p+2}). \quad (10)$$

Using the approximations of (10), the RK3-2L-IVS and RK4-2L-IVS methods are developed, which are simultaneously the 3rd and 4th order in time and 2nd order in space linear extrapolation numerical schemes. By using discrete data points within the vicinity of the cell faces, it is possible to find least squares gradient approximations at the cell centres [9]. Equation (11) is a truncated representation of the Taylor series:

$$\delta \mathbf{r} \cdot \nabla \xi(\mathbf{r}) \approx \xi(\mathbf{r} + \delta \mathbf{r}) - \xi(\mathbf{r}). \quad (11)$$

The above formula yields a system of linear equations that can be cast into matrix form as $\mathbf{A} \cdot \nabla \xi_p = \mathbf{d}$. The gradient that minimises $\|\mathbf{A} \cdot \nabla \xi_p - \mathbf{d}\|^2$ with respect to the inner product on \mathbb{R}^k can be obtained by solving the normal equations. The value of k equals the number of neighbouring nodes utilised to obtain the gradient at the p^{th} cell. In this paper, the gradients were constructed using only adjacent cells of ζ_p (ie. $k=6$). As a consequence, the gradients of the electric and magnetic fields can be used to approximate the + and - characteristics at the cell faces. Using these gradients, equation (12) establishes a 2nd order approximation for the + and - states:

$$\xi_{p+\frac{1}{2}}^- = \xi_p + \delta' \cdot \nabla \xi_p, \quad \xi_{p+\frac{1}{2}}^+ = \xi_{p+1} + \delta'' \cdot \nabla \xi_{p+1}. \quad (12)$$

In equation (12), δ' and δ'' are the vectors from the nodes (p) to $(p + \frac{1}{2})$ and $(p+1)$ to $(p + \frac{1}{2})$, respectively (see Fig. 2). Subsequently, the methods that employ (12) are classified as RK3-2G-IVS and RK4-2G-IVS, depending on the time integration.

The various IVS methods can also be implemented without flux splitting. The techniques that do not utilise IVS are referred to as RK3(RK4)-2L and RK3(RK4)-2G methods, which are the 3rd (4th) order linear extrapolation and the spatial gradient approximations without intensity vector splitting, respectively.

Boundary Conditions

In this section, the perfectly conducting wall, the incident field and absorbing boundary conditions are treated. On a perfectly conducting wall, the following conditions need to be satisfied [10]:

$$\mathbf{n} \times \mathbf{E} = \mathbf{0}, \quad \mathbf{n} \cdot \mathbf{H} = 0. \quad (13)$$

On structured grids, (13) implies that the tangential components of the electric field at a perfectly conducting wall boundary are zero. Equation (13) also entails that the magnetic components that are normal to that conducting wall are continuous across that wall.

For the purpose of the implementation of the incident field boundary condition, a classical waveguide is depicted in Fig. 3. In the figure, S and F represent the scattered and full field regions inside a waveguide, respectively. Typically, a fictitious dielectric is introduced inside the scattered region to absorb any reflected backward travelling waves.

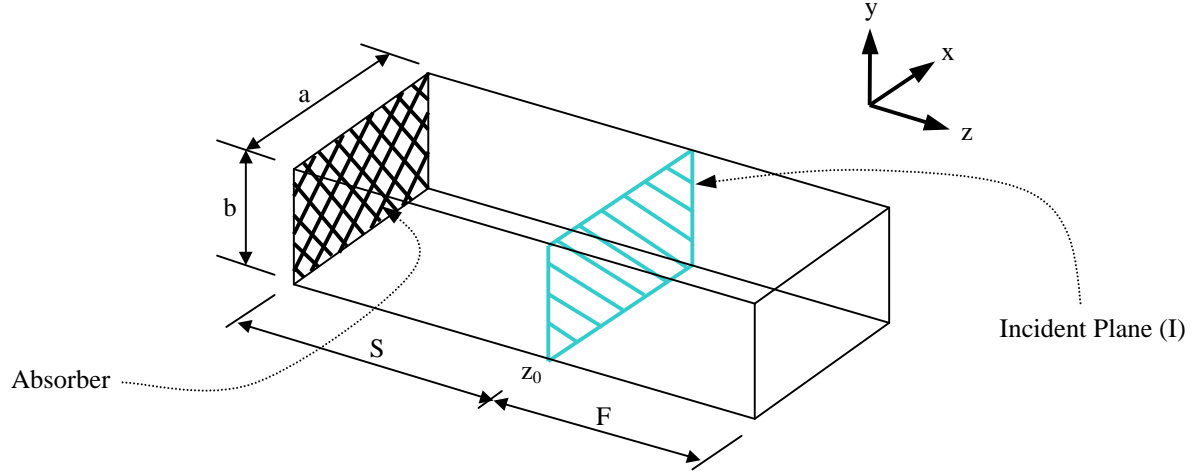


Figure 3. A waveguide with incident and absorbing boundary conditions.

In Fig. 3 it is assumed that z_0 represents the location where the incident field (I) is to be located. The scattered and full fields at the input plane can be obtained according to $F = S + I$. For the input plane, a continuous TE_{10} incident field is implemented as an incident boundary condition. Across the input plane, the scattered and full fields are computed according to the following incident field assumptions:

$$E_y^I = E_0 \sin\left(\frac{\pi x}{a}\right) \cos(\omega t - \beta_0 z_0), \quad (14a)$$

$$H_x^I = -\frac{\beta_0}{\omega \mu_0} E_0 \sin\left(\frac{\pi x}{a}\right) \cos(\omega t - \beta_0 z_0), \quad (14b)$$

$$H_z^I = -\frac{\pi}{\omega \mu_0 a} E_0 \cos\left(\frac{\pi x}{a}\right) \sin(\omega t - \beta_0 z_0), \quad (14c)$$

$$\beta_0 = \sqrt{\omega^2 \mu_0 \varepsilon_0 - \left(\frac{\pi}{a}\right)^2}.$$

In Fig. 3, an absorbing boundary layer is represented inside the scatter field region of the waveguide. In this work, a previously proposed Perfectly Matched Layer (PML) boundary condition [6] that has been adapted here for the use in the cell-centred schemes discussed in the previous section is used to absorb the waves inside the scattered region of the waveguide. The PML boundary condition is based on matching the impedance of the absorbing medium to the impedance of free-space. The PML boundary conditions are based on the following augmented Maxwell's equations:

$$\frac{\partial \mathbf{B}}{\partial t} + \mathbf{J}^* = \nabla \times \mathbf{E}, \quad \frac{\partial \mathbf{D}}{\partial t} + \mathbf{J} = -\nabla \times \mathbf{H}, \quad (15a)$$

where,

$$\mathbf{J}^* = \sigma^* \mathbf{H}, \quad \sigma^* = \frac{\mu_0}{\epsilon_0} \sigma. \quad (15b)$$

By satisfying (15b), the impedance of the PML equals that of free-space, and no reflections occur. From the reformulation of the Maxwell's equations, (1) is replaced by (15) in the discretisations, and new discrete in space equations are obtained for the numerical simulation of the electromagnetic behaviour within the absorbing material. Specific implementation details of the PML absorber will be outlined in future work, which will demonstrate the cell-centred finite-volume time-domain methods for the purpose of microwave heating.

Results

The waveguide of Fig. 3 is used as a case study to model and numerically simulate a Gaussian microwave pulse inside the apparatus. The full field region of the waveguide is truncated via a short-circuit, and the scattered field region employs the Petropoulos type PML boundary condition to absorb any backward travelling waves. The dimension of the waveguide is $a = 0.1\pi$, $b = 0.05\text{m}$ and $c = 0.4\text{m}$ (longitudinal dimension). At $z_0 = 0.1\text{m}$, the incident plane is excited using a TE_{10} 2.45GHz electromagnetic wave, with an average input power of 1W. The TE_{10} wave is multiplied by a Gaussian function to propagate a microwave pulse inside the waveguide:

$$\text{gauss}(t) = e^{-\frac{(2.5\frac{t}{T}-1)^2}{T}} \quad (16)$$

In equation (16), T represents the wave period inside the waveguide. The instantaneous electromagnetic fields were monitored over two periods. The domain of the waveguide is discretised into 54 000 (30 x 15 x 120) Cartesian cells. The time stepping of the numerical solvers is constrained by the relationship:

$$\Delta t = \frac{0.9}{c_{\max} \sqrt{\frac{1}{\delta x^2} + \frac{1}{\delta y^2} + \frac{1}{\delta z^2}}}.$$

where, c_{\max} is the maximum expected wave speed in the waveguide, and δx , δy and δz are the minimum mesh dimensions in the x , y and z coordinate directions [2].

Figures 4 and 5 show the results for the simulated TE_{10} Gaussian pulse using the numerical techniques discussed throughout the previous sections. Since it is well known that the FD-TD scheme is highly accurate, all of the established cell-centred numerical techniques have been compared to the FD-TD method to demonstrate the relative accuracy of each scheme. It is evident from the figures that the unstaggering of the unknowns introduces errors, and hence, higher order time marching schemes are required to better capture the FD-TD solution.

The introduction of intensity vector splitting smooths the noise that is apparent in the techniques that do not utilise IVS (see Figs. 4d and 5d). It is well-known that using higher order time integration techniques requires more computational effort to resolve the unknowns, and consequently, the techniques that employ IVS with RK3 and RK4 time integration are more computationally intensive than the FD-TD method. Although in this work, only the accuracy of the different cell centred schemes are compared, and times to compute the numerical solutions have been left to future investigations. It can be seen from figures 4 and 5 that the methods that make use of the gradients to approximate the + and – characteristics at the cell faces can capture the pulse as well as any of the other cell-centred numerical scheme discussed. Note that the results of RK4-2L-IVS have not been shown, since they were comparable to those obtained using RK4-2G-IVS.

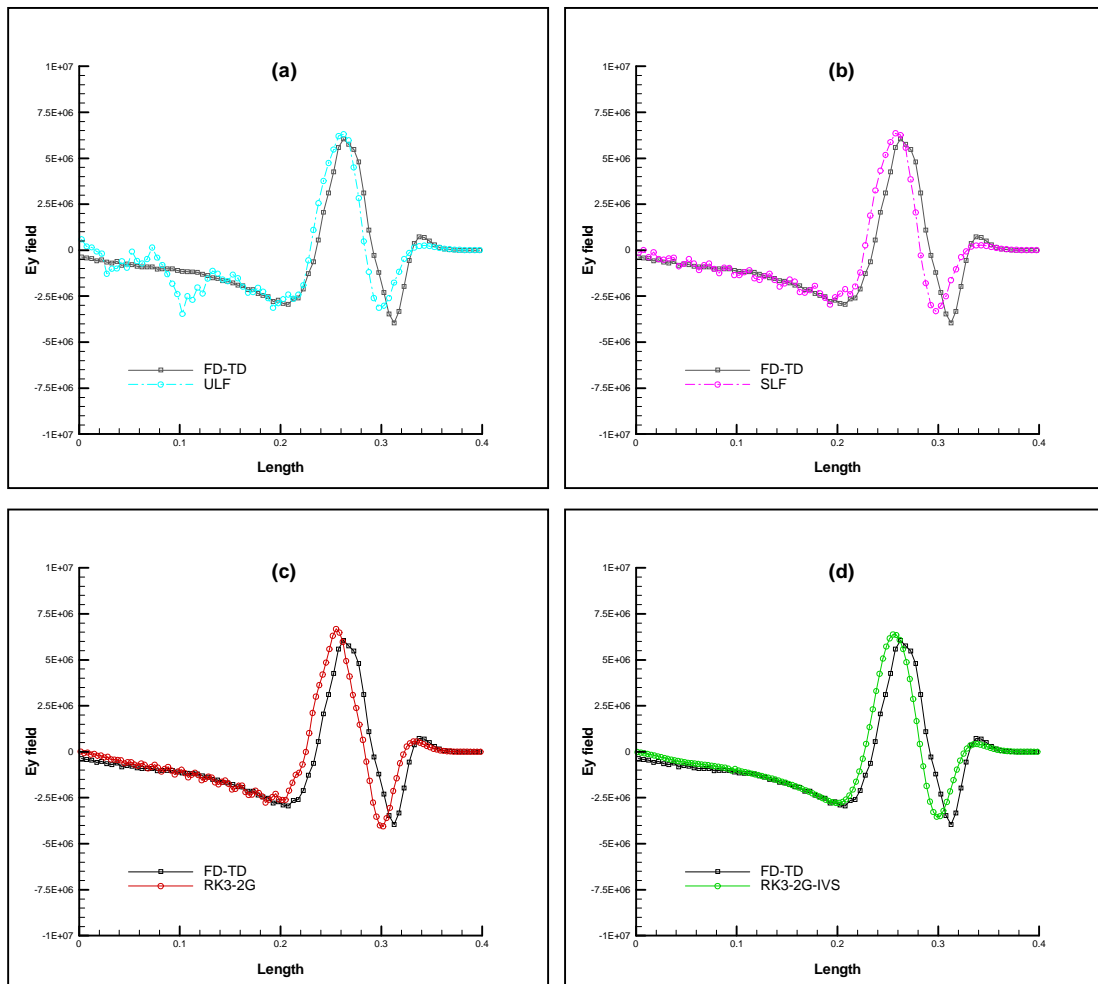


Figure 4. A two period pulse inside a TE_{10} waveguide; (a) ULF; (b) SLF; (c) RK3-2G; (d) RK3-2G-IVS

In Fig. 4a it is observed that the ULF scheme is conditionally unstable [4]. The RK4-1-IVS scheme, which utilises the 0th order extrapolation for the + and – characteristics, is highly dissipative as observed by Liu [4]. It is evident that first order spatial discretisations inadequately capture the behaviour of the solution (Fig. 4a-b). However, it must be noted that such methods are able to capture the wave phase, but the amplitude is smeared considerably.

In figures 4 and 5, most of the methods are observed to be out of phase, when compared to the FD-TD method. In Fig. 5a the RK4-2L scheme that only works on structured grids seems to capture the wave phase. This is an artefact of the spatial discretisation, and to further investigate how the phase errors could be reduced, higher order spatial discretisations would have to be adapted to the previously outlined cell-centred schemes. Most of the schemes outlined in this paper exhibit wavefront amplitude errors, especially Fig. 5a. For the RK4-2L method this is because of the grid used in the approximation of the cell face unknowns is four grid cells wide. Hence, as the incident field is propagated, the apparent noise due to the introduction of the microwave energy is propagated with the pulse. Such noise could possibly be reduced by smoothly introducing the incident field at the input boundary plane. This can be achieved through the superposition of a Gaussian function on the applied incident field.

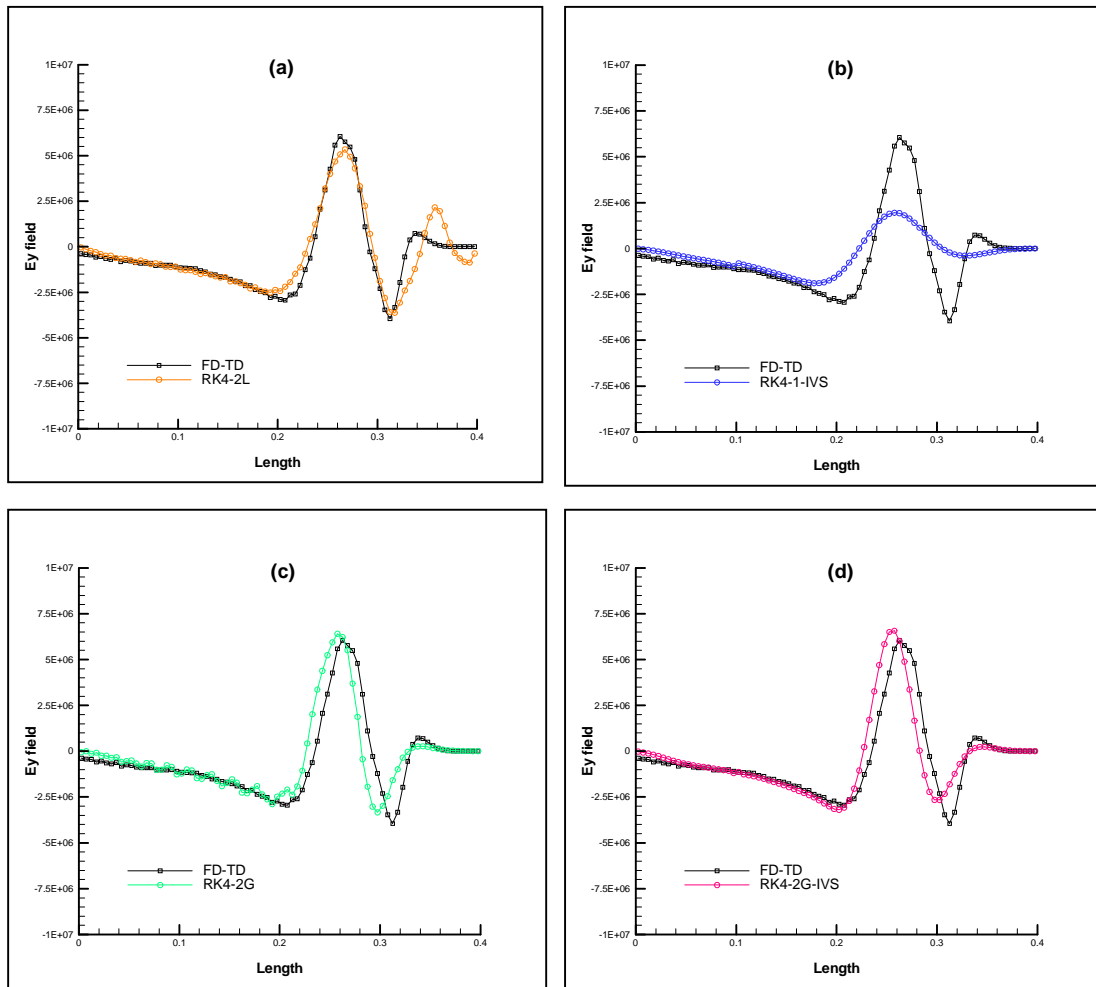


Figure 5. A two period pulse inside a TE_{10} waveguide; (a) RK4-2L; (b) RK4-1-IVS; (c) RK4-2G; (d) RK4-2G-IVS

Conclusion

In this work, cell centred time domain solvers for the Maxwell's equations were investigated and a number of solution strategies have been applied to resolve the Gaussian pulse

waveguide study. The governing equations were discretised using non-traditional techniques to obtain a surface-volume representation that was solved numerically using a number of different strategies. It is well known that the FD-TD method is very accurate, but it is not easily migrated to unstructured domains. A number of cell-centred schemes have been formulated for unstructured domains, but were implemented on structured domains so that they could be compared to the classical FD-TD method. Further research in the area will demonstrate how these schemes can be implemented on completely unstructured grids.

Leapfrog staggered and unstaggered time integration techniques were used to time march the discrete surface-volume representation of Maxwell's equations. When intensity vector splitting was introduced, the results appeared to be smooth, and the apparent noise evident in the schemes that did not utilise IVS was removed. This reduction in noise was due to the damping that these techniques induced in the numerical solution. The work clearly showed that unstructured time domain cell-centred Maxwell's equations numerical solvers on structured grids have produced reasonable results for the staggered in time leapfrog scheme (SLF). It was observed also that the Runge-Kutta based methods, with and without intensity vector splitting produced results that were comparable to the classical FD-TD method.

For the purpose of microwave heating, future research will analyse in more detail the effect that a lossy material can have on the electromagnetic phenomenon evolving on the grid which has unknowns located at the cell centres. In that work, more rigorous tests are to be conducted regarding dispersion and dissipation errors.

Acknowledgments

The authors would like to thank Dr. Huawei (Bob) Zhao for his input into the development of this paper. Also, many thanks to Dr. Joseph Young for his help with the visualisations in the accompanying presentation.

References

1. Dibben, D.C. and A.C. Metaxas, *Time Domain Finite Element Analysis of Multimode Microwave Applicators Loaded with Low and High Loss Materials*. Intl. Conf. Microwave and High Energy Heating, 1995. **1-3.4**.
2. Zhao, H. and I. Turner, *An analysis of the finite-difference time-domain method for modelling the microwave heating of dielectric materials within a three-dimensional cavity system*. Journal of Microwave Power and Electromagnetic Energy, 1996. **31**(4): p. 199-214.
3. Madsen, N.K. and R.W. Ziolkowski, *A three-dimensional modified finite volume technique for Maxwell's equations*. Electromagnetics, 1990(10): p. 147-161.
4. Liu, Y., *Fourier Analysis of Numerical Algorithms for the Maxwell Equations*. Journal of Computational Physics, 1996. **124**: p. 396-416.
5. Yee, K.S., *Numerical Solution of Initial Boundary Value Problem Involving Maxwell's Equations in Isotropic Media*. IEEE Trans. Antennas Propagat., 1966. **14**: p. 302-307.

6. Petropoulos, P.G., L. Zhao, and A.C. Cangellaris, *A Reflectionless Sponge Layer Absorbing Boundary Condition for the Solution of Maxwell's Equations with High-Order Staggered Finite Difference Schemes*. Journal of Computational Physics, 1998. **139**: p. 184-208.
7. Madsen, N.K. and R.W. Ziolkowski, *Numerical solution of Maxwell's equations in the time domain using irregular nonorthogonal grids*. Wave Motion, 1988(10): p. 583-596.
8. Taflove, A., *Re-inventing Electromagnetics: Supercomputing Solution of Maxwell's Equations Via Direct Time Integration on Space Grids*. AIAA paper 92-0333, 1992(New York).
9. Barth, T.J., *Aspects of Unstructured Grids and Finite-Volume Solvers for the Euler and Navier-Stokes Equations*. Lecture Notes Presented at the VKI Lecture Series, 1994-05, 1995.
10. Collin, R.E., *Field Theory of Guided Waves*. 1960: McGraw-Hill Book Company.